Journal of Alloys and Compounds 986 (2024) 174102

Contents lists available at ScienceDirect

Journal of Alloys and Compounds

journal homepage: www.elsevier.com/locate/jalcom

Ultrafast high-temperature sintering (UHS) of WC and WC-containing ZrB_2

Emanuele De Bona [a,*], Levent Karacasulu [a,b], Cekdar Vakifahmetoglu [b], Vincenzo M. Sglavo [a,c], Mattia Biesuz [a,c,**]

[a] Department of Industrial Engineering, University of Trento, Via Sommarive 9, Trento, TN 38123, Italy
[b] Department of Materials Science and Engineering, Izmir Institute of Technology, Urla, İzmir 35430, Türkiye
[c] INSTM, Via G. Giusti 9, Firenze, MI 50121, Italy

ARTICLE INFO

Keywords:
ZrB_2
WC
Ultrafast high-temperature sintering
UHS
Ultra high-temperature ceramics

ABSTRACT

WC and ZrB_2 are refractory ceramics with excellent thermophysical properties and melting temperatures exceeding 2800°C. Both materials require the application of external pressure and long sintering times for their consolidation. In particular, commercially available ZrB_2 powders are intrinsically difficult to sinter and usually need long pre-processing steps such as high-energy ball milling. Ultrafast high-temperature sintering (UHS) is a recently developed technique that enables the consolidation of bulk ceramics within minutes. In the present work, pure WC was efficiently densified to above 98% in just 3 min by UHS. Moreover, small WC additions enhanced ZrB_2 densification by activating liquid phase sintering. Samples containing 5 and 10 vol% WC were sintered to 95 and 96%, respectively, in 2 min. All the WC initially present in the blend reacts to form a liquid phase during sintering and solidifies as WB and (Zr,W)C upon cooling. The formation of a ZrB_2-(Zr,W)B_2 core-shell structure was detected in all the sintered composites. The hardness of UHS samples reaches 15 GPa (WC - ZrB_2 composites) and 21 GPa (pure WC), similar to that measured in materials obtained by slower and more sophisticated pressure-assisted sintering techniques.

1. Introduction

Ultra-high temperature ceramics (UHTC) are a broad family of inorganic refractory compounds [1]. They find application in extreme environments thanks to their resistance to chemicals, wear, radiation, and mechanical loads, even at high temperatures. UHTC are identified as compounds possessing melting points exceeding 3000°C, thus including transition metal borides, nitrides, and carbides [2–4].

One of the most interesting UHTC is zirconium diboride (ZrB_2) owing to its high melting point (3250°C), hardness (23 GPa), and elastic modulus exceeding 500 GPa [5–7]. While being predominantly covalently bonded, it exhibits a strong metallic character, which leads to high thermal ($\geq$ 60 W/mK) and electrical (10^7 S/m) conductivities at room temperature [5–7]. Due to its relatively low density (6.08 g cm^{-3}), ZrB_2 is of particular interest for lightweight applications, including aerospace and defense [8,9]. However, pure ZrB_2 is extremely hard to sinter: while covalent bonds are pivotal for its refractory properties, they also hinder diffusion and densification [2,7,10,11]. As such, ZrB_2 typically requires prolonged and expensive sintering procedures aided by external pressure like hot pressing (HP)[9] or spark plasma sintering (SPS)[12]. This determines some substantial limitations, the productivity of SPS and HP being relatively low compared with pressure-less sintering. Moreover, such technologies can be poorly integrated with complex shapes and are mostly used to obtain monoliths with simple geometries. In addition, the applicability of single-phase ZrB_2 for high-temperature environments is restricted due to its poor oxidation and ablation resistance, as well as its limited damage tolerance[8]. Considering the aforementioned difficulties, several additives as sintering aids such as B_4C [13–15], C [14–16], transition metals (e.g., Fe and Cr) [17], $MoSi_2$ (and the other silicides) [18–22], Si_3N_4 [23], W [24], SiC [25], WC and various carbides [5–7,13,26] have been shown to improve the pressure-less sintering behavior of ZrB_2.

Among the candidates, WC exhibits exceptional performance as a sintering aid because it not only facilitates the densification of ZrB_2 but also enhances the mechanical properties at elevated temperatures [24,27]. During sintering of WC-ZrB_2 composites, WB forms, and WC reacts with the oxide layer on the surface of the diboride grains. WB softens or melts at high temperatures and aids densification by liquid phase

* Corresponding author.
** Corresponding author at: Department of Industrial Engineering, University of Trento, Via Sommarive 9, Trento, TN 38123, Italy.
E-mail addresses: emanuele.debona@unitn.it (E. De Bona), mattia.biesuz@unitn.it (M. Biesuz).

https://doi.org/10.1016/j.jallcom.2024.174102
Received 8 November 2023; Received in revised form 7 February 2024; Accepted 6 March 2024
Available online 7 March 2024

sintering [28–32]. Moreover, the addition of WC to ZrB_2 can cause anisotropic grain growth [29]. WC doped-ZrB_2 exhibits high flexural strength at elevated temperatures probably due to the oxygen-free grain boundaries formed while sintering [2,24,33]. In addition, WC addition enhances the oxidation resistance of the composite compared to pure ZrB_2 [24,31,34,35].

Densification of ZrB_2 by conventional sintering - even using sintering additives - requires anyway long times (i.e., $\geq$ 2 h) at extreme temperature, resulting in grain coarsening which can also impact the mechanical properties [7]. Consequently, non-conventional sintering techniques have been studied to reduce the sintering time and/or temperature. These include hot pressing [7,36–41], reactive hot pressing [42–46], spark plasma sintering (SPS) [7,36,47,48], flash spark plasma sintering (FSPS) [49], and ultrafast high-temperature sintering (UHS) [11,50].

UHS is a pressureless sintering technique introduced by Wang et al. in 2020 [51]. It allows the densification of ceramics by radiative very rapid heating (10^3 – 10^4 K/min), usually under an inert atmosphere (Ar) in extremely short times (10 – 300 s) [51,52]. This is attained by introducing the green pellet within a highly porous graphite felt, which is quickly Joule heated being crossed by an electrical current. UHS has already been employed on different ceramic systems including oxides [53–57] and covalent refractories [58–61]. When commercial ZrB_2 powder was sintered via UHS under Ar gas, pure ZrB_2 resulted in a relative density of 84%, while densities up to 98% were obtained with the addition of B_4C (10 wt%) [11]. In another study, UHS under vacuum allowed to reach a final relative density of 93% [50].

The present work aims to investigate the UHS densification of composites in the WC – ZrB_2 system and analyze the effect of processing parameters on the microstructure and phase evolution of the sintered bodies.

2. Experimental procedures

2.1. Samples preparation

ZrB_2 powder from Höganäs (Grade B, D_{50} = 1.5–3 μm) and WC powder from Inframat Advanced Material (particle size 150–200 nm and crystallite size 40–70 nm) were used in the present investigation. Mixtures containing 5, 10, 25, and 50 vol% WC were prepared by ultrasonic mixing for 30 min in methylethylketone and then dried overnight at 150°C. Also, pure WC and ZrB_2 powders were considered. The green bodies were shaped by uniaxial pressing using a 6 mm diameter steel die under 500 MPa. The volume of the disks was kept constant (thickness = 1 mm), the mass of the samples clearly increasing with WC content.

The UHS setup has already been described in previous publications [11,52]. The sintering treatments were performed within a 6×15×30 mm^3 graphite felt (Sigratherm® GFA). Such size was chosen as it allows a flat temperature profile in the central region of the felt, where the samples are placed by opening a hole in the felt. All disks were sintered under inert Ar atmosphere. The current was applied using an Agilent 6674 A power supply (maximum 35 A and 60 V), operating in current control (i.e., the applied voltage was lower than the set voltage limit). For every composition, treatments of 60 s under 30 A, 32.5 A, and 35 A were performed. When samples did not melt, additional 120 s and 180 s UHS treatments were performed to increase the final density. During sintering, the applied voltage reached a plateau between 13 and 17 V depending on the set current and sintering time. Such behavior has been already studied in detail and reported in a separate work [52]. The processing conditions were selected based on our previous experience with the ZrB_2-B_4C system[11].

2.2. Characterization

The true density of the samples was measured by He pycnometer using an Ultrapyc 5000 (Anton Paar) on pure powders and ZrB_2-WC powder mixtures. The apparent density of the sintered pellets was evaluated by Archimedes' method (ASTM C 830 norm) and then converted into relative density using the pycnometer data. The measured true densities of the pure compounds (6.08 g cm^{-3} for ZrB_2, 15.58 g cm^{-3} for WC) were found to be in good agreement with the literature values [10,62] (within the possible error generated by the limited degree of surface oxidation for the nanometric WC powders), while the composites were respecting the rule of mixtures (6.56 g cm^{-3}, 7.02 g cm^{-3}, 8.44 g cm^{-3} and 10.79 g cm^{-3} for the 5, 10, 25 and 50 vol% WC, respectively).

Microstructural characterization was performed both on polished and fracture surfaces by using a JEOL (model JSM-5500) scanning electron microscope (SEM). Being ZrB_2 and WC both electrically conductive, no preliminary metallization was required. Energy-dispersive X-ray spectroscopy (EDXS) linescans and mappings were recorded separately on a JEOL JSM-IT300 LW SEM equipped with a Bruker XFlash 630 M detector operating at 20 keV.

X-ray diffraction (XRD) analysis was performed on polished surfaces using a Rigaku IIID Max diffractometer equipped with Cu-K_α (λ = 1.5405 Å) X-ray source (40 kV; 30 mA). Rietveld refinement on the diffraction patterns was carried out with the software package Jana2006 [63]. The data used for the refinements are all accessible on the Crystallographic Open Database and can be found for ZrB_2[64], WC [65], WC_{1-x}[66], W_2C [67], WB [68], and ZrC [69].

Vickers hardness was measured on polished samples (using SiC paper up to grit 4000) by a Future-Tech FM-310 microhardness tester under load of 9.8 N. Each value reported here is the average of ten measurements.

3. Results and discussion

The relative density of the sintered samples is reported as a function of the applied current in Fig. 1. Black, grey and light grey points refer to treatments performed for 60 s, 120 s, and 180 s (only for pure WC), respectively. The results are also summarized in Table S1.

Treatments under 30 A caused almost no densification for all compositions. As expected [11], pure ZrB_2 does not achieve full densification even in harsh UHS conditions (87% under 35 A for 120 s). The addition of WC enhances the sinterability within certain compositional limits: composites containing 5 and 10 vol% WC overtake 95% relative density in only 120 s under 35 A. On the other hand, loads above 10 vol% led to lower densities or sample melting. The samples containing 25 and 50 vol % melted for currents in excess of 32.5 A. Remarkably, also pure WC shows good sinterability by UHS, reaching 90% relative density in 60 s under 35 A, and exceeding 98% after 180 s.

A direct measurement of the sintering temperature was not possible in the available UHS setup, but an estimate was performed by FEM as reported in another work where the same device and sintering conditions were used [11]. In summary, the modeled maximum sample temperature under 35 A ranges between 2250 and 2350°C, while the felt can heat up to 2600°C depending on the type of contact with the sample. Some tests were performed to assess the reliability of such models and B_4C (T_m = 2350°C) was really melted in said conditions, thus confirming that the sample temperature under 35 A was equal to or higher than 2350°C.

The microstructure of all samples produced under 35 A is shown in Fig. 2. In addition, also the 25 vol% WC sample produced at 32.5 A for 60 s is shown since it reached a relative density >90% (note that "catastrophic melting" with partial loss of the shape was observed under 35 A for the 25 vol% and 50 vol% WC pellets). In agreement with previous findings [2,7,10,11], pure ZrB_2 undergoes limited densification accompanied by coarsening phenomena, which can be especially detected after the 120 s treatment.

The WC addition leads to changes in the sintering mechanism, with some composites showing evidence of liquid phase sintering. The formation of the liquid phase is evident in the 10 vol% WC samples after 60

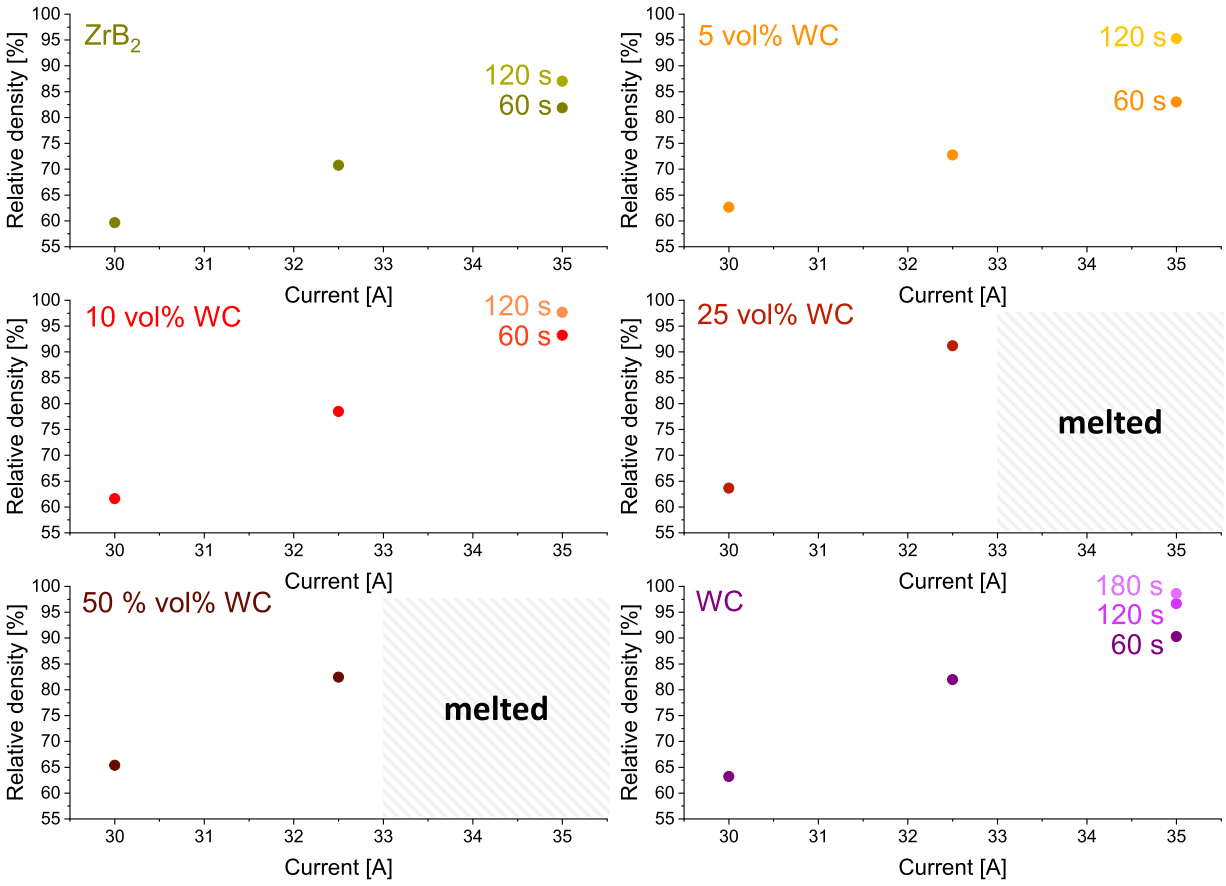

Fig. 1. Relative density of the ZrB_2 – WC sintered disks as a function of the applied current during UHS. Black, grey, and light grey points refer to treatments performed for 60 s, 120 s, and 180 s, respectively. The shaded regions correspond to conditions leading to the sample melting.

and 120 s; in particular, one can observe the development of an intergranular "phase" wetting the grain boundaries of the big diboride grains (additional micrographs are available in the supplementary material, Figs. S1–3). The liquid phase formation can also be seen for the 5 vol% WC composition after 120 s (Fig. S1). Conversely, after 60 s the microstructure does not provide definitive evidence about the formation of a liquid phase. The micrographs well agree with the density measurements: the 10 vol% WC samples show an improvement of the final density of about 10 vol% WC compared with pure ZrB_2 for both 60 and 120 s UHS under 35 A. On the other hand, the addition of 5 vol% WC is not very effective for 60 s treatments, while it is beneficial for the 120 s UHS process. In fact, the 5 vol% WC composites show a marginal density improvement after 60 s (≈+1.2% compared with pure ZrB_2), but the densification is remarkably enhanced after 120 s (≈+8.2% compared with pure ZrB_2). Therefore, the formation of the liquid phase between 60 and 120 s under 35 A, as evidenced by SEM, seems the main origin of the enhanced densification of the composites. Finally, SEM micrographs confirm the excellent densification of binderless WC by UHS in only 3 minutes.

Upon sintering, WC and ZrB_2 react to form new phases, responsible for the liquid phase sintering. A combination of XRD and EDXS analyses was used to determine the final composition of the sintered samples. Fig. 3 shows the backscattered electrons SEM images (left column) of the densest sample of each composition, alongside the EDXS mapping of W (central column) and Zr (right column). The chemical composition (in terms of W and Zr, thus excluding B and C whose quantification is cumbersome) of the different phases found by EDXS is summarized in Table 1. XRD patterns of the samples sintered at the highest currents (32.5 A for 25 vol% WC, 35 A for all the other compositions) are shown in Fig. 4 and the results of the Rietveld refinements are reported in Table 2.

Unsurprisingly, pure ZrB_2 XRD pattern shows the presence of one single crystalline phase identified with hexagonal ZrB_2 ($a = b = 3.169$ Å, $c = 3.531$ Å; $\alpha = \beta = 90°$, $\gamma = 120°$). Pure WC is characterized by the presence of the hexagonal phase ($a = b = 2.908$ Å, $c = 2.873$ Å; $\alpha = \beta = 90°$, $\gamma = 120°$) and two secondary phases (visible in Fig. 4**B**): face centred cubic (FCC) WC_{1-x}[66,70,71] (< 3.5%vol; $a = b = c = 4.208$ Å; $\alpha = \beta = \gamma = 90°$) and ε-$W_2C$[67] (< 1%vol; $a = b = 5.162$ Å, $c = 4.724$ Å; $\alpha = \beta = 90°$, $\gamma = 120°$). In all composites, WC appears to be consumed entirely during sintering treatment with the formation of two new phases and the alteration of the ZrB_2 matrix [26]. The composition of the sintered samples is discussed in the following lines, where the phases are listed according to the order in which they are numbered in Fig. 3 (middle row):

1. White phase: near-stoichiometric WB. The formation of this phase is reported in the literature for WC–doped ZrB_2 when the solubility of W in ZrB_2 is exceeded [26,34]. The extremely low lattice deformation implies negligible Zr or C contamination, as confirmed by the very small Zr signal in EDXS mapping (likely coming from the surrounding grains). Some reflections of WB are already visible in the 5 vol% WC diffraction patterns, but their intensity is so limited that its quantification is quite complicated (< 1 vol%). This issue is also in good agreement with the literature, where such phase was found to form when the nominal solubility limit of about 8 mol% W in ZrB_2[34] is exceeded (the theoretical 5 vol% WC corresponds to 7.6 mol%).
2. Grey phase: mixed FCC carbide $(Zr,W)C_{1-x}$. The presence of a limited amount (1%) of FCC phase starts being detectable already for the 5 vol% WC sample, especially after 120 s at 35 A (Fig. 4). ZrC

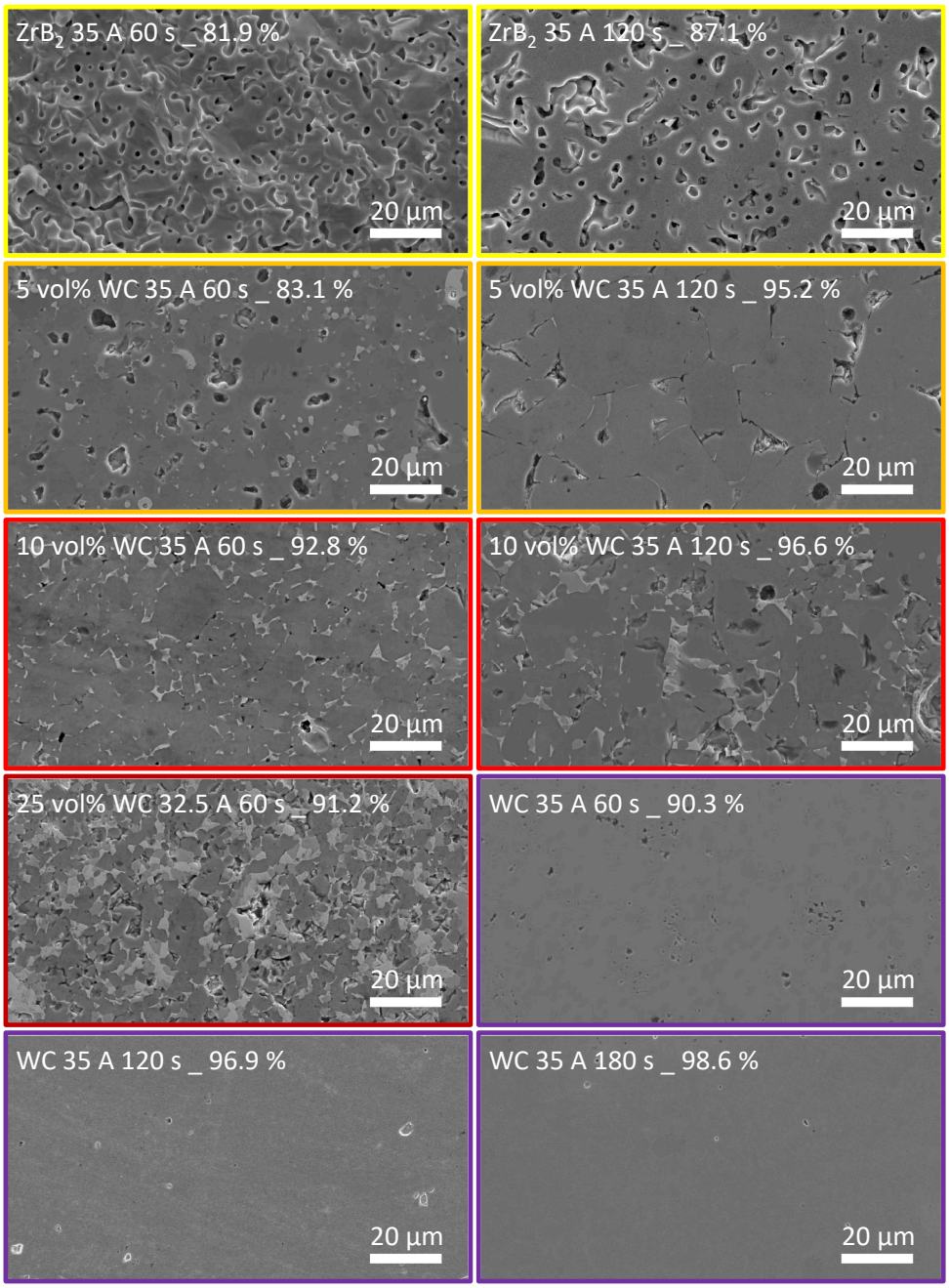

Fig. 2. SEM images of the polished surface of the samples produced at 35 A and the 25 vol% WC sample produced at 32.5 A for 60 s. The used processing conditions and the relative density are reported.

(4.71 Å)[72], WC_{1-x} (4.37 Å)[66,70], and the theoretically possible ZrB (4.65 – 4.9 Å)[73,74] are all FCC with a structure derived from rock salt. Their lattice parameters are significantly different from that of the phase found in the present work (Table 2), which can be identified as a mixture of two or more of these compounds. The high-temperature (> 1000°C) cubic (W,Zr)C solid solutions is reported extensively in the literature [75–77], although their crystallographic characterization is generally limited. Large nonstoichiometric domains are documented for both ZrC_{1-x}[72] and FCC WC_{1-x}[66,70,71]. Similarly, the stability of ZrB should be confined to $T > 800$°C [78] or upon extremely slow cooling, but it can be extended by the presence of C [74].

The mixed carbide phase composition can be assessed starting from the EDXS data. The W/(W+Zr) weight ratio settles to 0.4 (i.e., about 0.2 vol ratio and 0.3 mol ratio). If one considers an ideal solid solution of stoichiometric $ZrC_{1.0}$ and cubic $WC_{1.0}$[79], a lattice constant of 4.608 Å is obtained, similar to the values found in this work. Such value is in good agreement with the calculation proposed by Jia et al. for the lattice parameter of (W,Zr)C solid solutions [80].

The remaining discrepancy with the experimental value (about 0.02 Å) falls within the range of uncertainty of the literature values for pure ZrC. Such deviation could be explained either by taking into account the substoichiometry of the mixed carbide, i.e., $(Zr,W)C_{1-x}$, or with the effect of substitutional B (or both), but this goes beyond the scope of this publication.

3. Dark phase: ZrB_2-based core-shell structure. The formation of (Zr,W)B_2 solid solution from the reaction between WC and ZrB_2 is extensively documented in the literature [24,27,34,81], similiraly to what happens from the interaction with other carbide systems [82,83]. However, only a few authors reported the formation of a core-shell

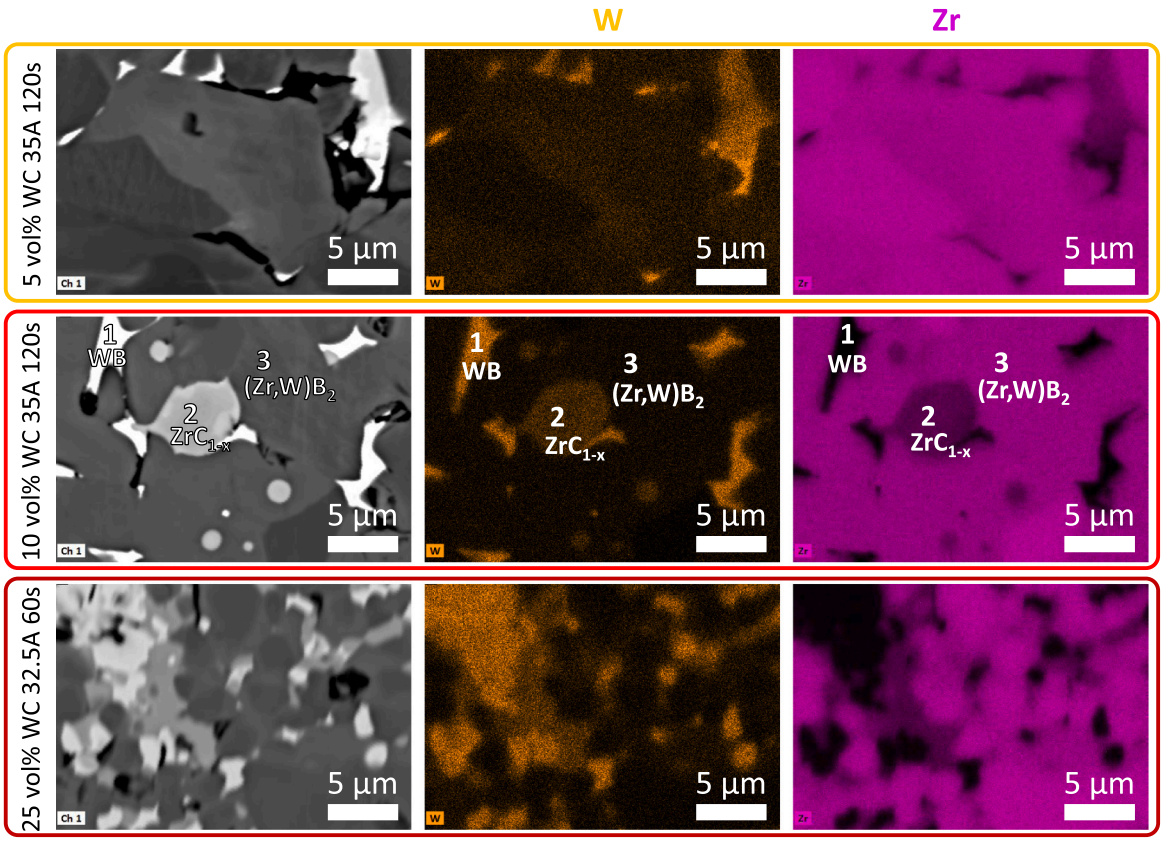

Fig. 3. Backscattered electrons SEM images and EDXS maps (W and Zr) of the densest samples of each composition (35 A 120 s for 5 and 10 vol% WC, and 32.5 A 60 s for 25 vol% WC).

Table 1
Average W content (in wt%) in the different phases (numbered as in Fig. 3) as measured by EDXS. The relative amount does not account for B and C.

	5 vol% WC	10 vol% WC	25 vol% WC
1. White	> 99	> 99	> 99
2. Grey	40.8 ± 1.2	42 ± 0.7	43.2 ± 1.1
3. Dark _ shell	8.2 ± 0.7	10.4 ± 0.9	12.3 ± 0.8
3. Dark _ core	< 0.5	< 0.5	< 0.5

structure [26,40,43,84]. Moreover, the solubility of W in ZrB_2 presents a large scatter depending on the sintering conditions (temperature and atmosphere) and the chemical nature of the additives (W or WC; presence of B_4C and/or graphite). Overall, while many studies report a nominal composition beyond which W-based phases precipitate along the $(Zr,W)B_2$ matrix, little attention has been paid to the actual W amount in the $(Zr,W)B_2$ solid solution grains. Khadimallah et al. [27] performed a combined experimental and atomistic approach to find the solubility limit of 3 at% W in ZrB_2 at 2100°C, the value being negligible below 1380°C. However, the sintering conditions of their work differ significantly from the largely out-of-equilibrium conditions of the present study.

In the present work, the formation of two (or more) distinct $(Zr,W)B_2$ phases can be obsered by both SEM-EDXS (Fig. 5) and XRD (Fig. 4**C**). Penetration of W into the ZrB_2 grains can be observed by the EDXS lines (Fig. 5**B**), where the two regions show distinctly different W content. The transition between the two regions also seems quite sharp from the backscattered electron image (Fig. 5 **A**). Consistently, XRD show peak shifts to higher angles for the ZrB_2-based phase (i.e., a lattice parameter reduction due to the substitution of W for Zr, whose atomic radii are 135 and 160 pm respectively[85]), but also peak splitting. This supports the evidence of the formation of two (or more) distinct $(Zr,W)B_2$ solid solutions with different W contents. Two aspects are worth to be pointed out:

i. for all samples, the more distorted phase is also the most abundant one (in vol%);
ii. the lattice parameter variation is for both phases beyond that reported in the literature, thus indicating a W contents well above 3 mol% in the shell.

These findings do not contradict the literature solubility values nor what stated about WB formation (phase 1 in Fig. 3, and point 1. in this list). The W content exceeds the theoretical one calculated by Khadimallah et al. [27] only in the shell part. When the sintering time is increased (from 60 to 120 s), the shell volume fraction increases and its distortion (i.e., the W content) decreases. The diboride grain shell composition therefore shifts towards the theoretical equilibrium solubility value. The total W content considering both the core and the shell of the $(Zr,W)B_2$ phase always sits around the overall nominal 8–10 mol% solubility limit [34], beyond which secondary phases start developing and/or W dissolves in ZrC.

To summarize, the exceptionally high temperatures reached in UHS allow the dissolution of a significant amount of W in the ZrB_2 matrix. The high cooling rate instead "freezes" the penetration front of W in the ZrB_2 grains, thus creating the core-shell structure. The amount of WB formed and W dissolved in ZrC is dictated by the sintering temperature and the solubility of W in ZrB_2 at such temperature.

From the microstructures of Fig. 5 **A and** Figs. S1–3, it appears that both WB and (W,Zr)C are responsible for liquid phase sintering. Nevertheless, the pure and stoichiometric compounds (ZrC [86], WC [71], WB [87]) all melt above 2600°C. Some systems involved in the present work, such as Zr-W-B, W-B-C, or Zr-B-C have been extensively studied [88,89], but nothing has been published on the quaternary system Zr-W-C-B, yet. Due to the extremely different particle size (3 µm

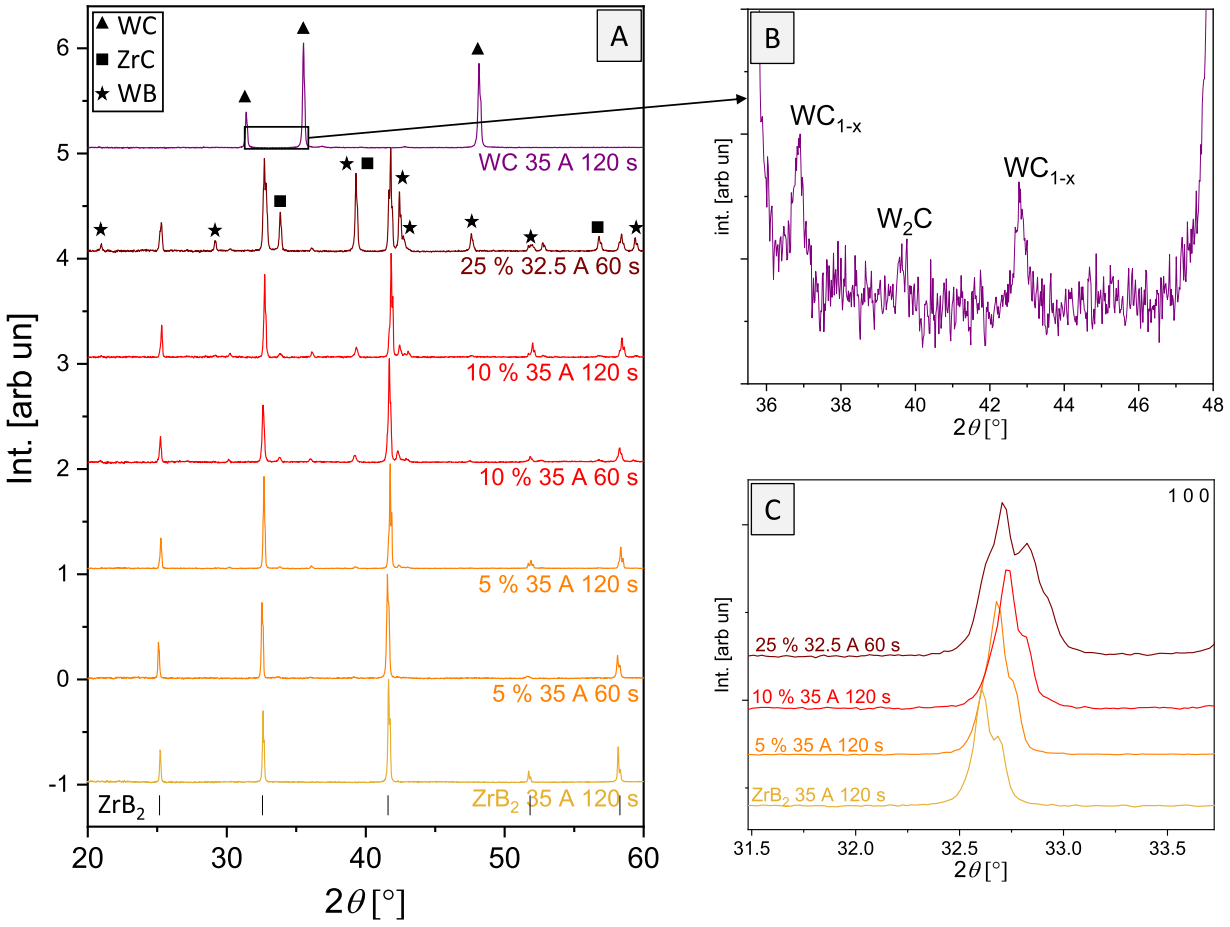

Fig. 4. (A) XRD spectra of the samples sintered in the harshest conditions (32.5 A for 25 vol% WC and 35 A for the others), including pure ZrB_2 and WC; (B) peaks of secondary phases present in pure WC; (C) peak shift and splitting of the (1 0 0) reflection of the $(Zr,W)B_2$ phase in the mixed samples.

Table 2
results of the Rietveld refinements performed on the XRD patterns shown in Fig. 4. *The remaining 4% is constituted of W_2C and WC_{1-x}, not included in the table for the sake of readability.

	Phase fraction [vol%]					Lattice constants [Å]						
						ZrB_2		$(Zr,W)B_2$		(Zr,W)C	WB	
	ZrB_2	$(Zr,W)B_2$	WB	ZrC	WC	a	c	a	c	a	a	c
ZrB_2 35 A 120 s	100					3.169	3.531					
5 vol% WC 35 A 60 s	24	73	< 1	1		3.167	3.534	3.161	3.521	4.588		
5 vol% WC 35 A 120 s	4	95	< 1	1		3.167	3.531	3.162	3.525	4.585		
10 vol% WC 35 A 60 s	18	75	3	4		3.166	3.533	3.154	3.511	4.582	3.113	16.934
10 vol% WC 35 A 120 s	14	78	3	5		3.166	3.528	3.161	3.518	4.581	3.108	16.894
25 vol% WC 32.5 A 60 s	29	40	13	18		3.166	3.529	3.156	3.513	4.579	3.108	16.894
WC 35 A 120 s					96*							

for ZrB_2 vs. 200 nm for WC) and the abrupt sintering schedule, it is likely that the chemical equilibrium was not reached throughout the samples, if not just locally. On the surface of the ZrB_2 grains, where the reactions between WC and ZrB_2 can take place, the WC-ZrB_2 mixture composition can differ significantly from the nominal one, giving rise to low melting compounds. Substoichiometric ZrC_{1-x} and ZrB_{2-y} melt at lower temperatures than the stoichiometric compounds and a broad L + $ZrC_{1(-x)}$ + $ZrB_{2(-y)}$ domain is present in the Zr-B-C system below 2300°C [88–90]. Similarly, in the W-C-B system, a slight deviation from stoichiometry combined with B addition lowers the melting point of WC below 2350°C [89]. The liquid phase during sintering was likely a W-Zr-B-C mixed composition that later solidified into WB and (Zr, W)C upon cooling [26]. Moreover a clear eutectic solidification microstructure can be noticed in between the primary diboride grains (Fig. S2). Such lamellar structure includes the WB and W-substituted ZrC_{1-x} phases. Unfortunatelly, the pseudobinary phase diagram WB-ZrC is not available to the best of our knowledge; however, the microstructural evidences suggesting an eutectic reaction between these compouds seems robust.

Fig. 6 reports the hardness of the densest sample for each composition (60 s at 32.5 A for 25 vol% WC, 120 s at 35 A for the other mixtures). ZrB_2-WC composites reach around the same hardness regardless their density or composition (indentation imprint size = 32–37 μm). It is worth noting that the nominal WC content can be misleading, since this phase is absent in the final sintered samples. Both WB (30 GPa [91]) and ZrC (25.5 GPa [92]) are harder than ZrB_2 (15–23 GPa[5,93]), and should act as reinforcement. However, this occurs only if their volumetric fraction exceeds a certain threshold: works on ZrB_2–based composites with WC and/or B_4C as sintering aids do not show a clear

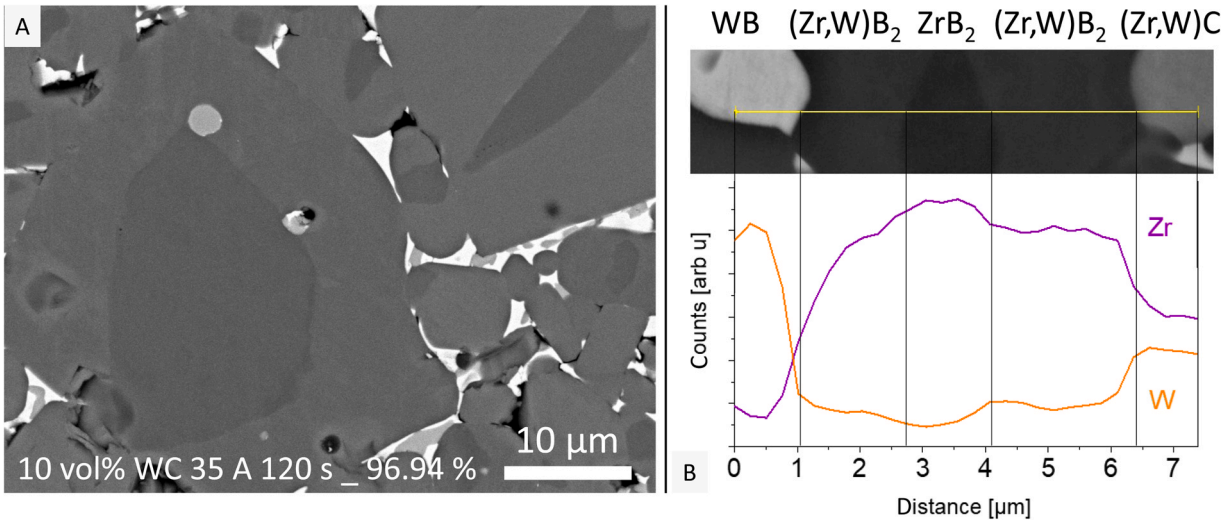

Fig. 5. (A) backscattered electrons SEM image of the 10 vol% WC sample sintered at under 35 A for 120 s; (B) linescan across the core-shell structure of a ZrB_2-based grain in the same sample.

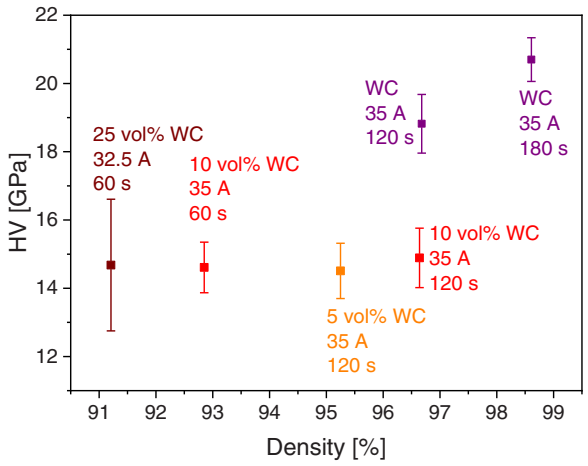

Fig. 6. Vickers hardness of the densest sample for each composition (32.5 A 60 s for 25 vol% WC, 35 A 120 s for 5 and 10 vol% WC) as a function of their density. Pure WC sintered at 35 A for 120 and 180 s is also included.

hardness trend for low dopant concentrations [5,93–96], the grain size being a more influencing factor with respect to density and/or dopant. Moreover, the hardness of ZrC_x strongly depends on its stoichiometry, exhibiting a maximum of 25.5 GPa for $ZrC_{0.86}$[97]. Samples with 5 and 10 vol% WC only contain a limited amount of WB and (Zr,W)C, so their hardness is around that of the ZrB_2 matrix (grain size 19.7±3.2 µm for 5 vol% WC and 9.8±2.1 µm for 10 vol% WC). The effect of porosity is also limited, as in both samples the pores are micron-sized pores and very localized. The situation is different in the 25 vol% WC sample: the density is significantly lower and the porosity finer and distributed evenly (grain size 4.5±0.7 µm); the presence of a large amount of WB and (Zr,W)C increases the hardness to about 15 GPa even if the relative density is only about 91%.

Pure WC (grain size 17.4±2.7 µm) instead exhibits excellent performance, matching the literature values for samples of comparable grain size produced by more time- and energy-consuming methods such as hot pressing (22.9–24.2 GPa) [98] or SPS (19.5–25.5 GPa) [62]. Such a result is of particular interest if one considers that, contrarily to pressure-assisted sintering, UHS can be integrated easily also with complex shapes.

4. Conclusions

The combination of ultrafast high-temperature sintering (UHS) and WC addition was proven to be successful in producing highly dense (>95%) ZrB_2-based ceramics within minutes. The activation of a liquid phase sintering process upon 2 min long UHS allows to obtain ~95% dense ZrB_2-5 vol% WC and ~97% dense ZrB_2-10 vol% WC. Higher WC content yields ~91% dense samples in 1 min at 32.5 A in ZrB_2-25vol% WC but leads to melting for higher currents or sintering times.

During UHS, all WC is consumed to form WB, (Zr,W)C, and a (Zr,W)B_2-ZrB_2 core-shell structure in the diboride matrix. UHS was revealed to be also highly efficient for the densification of pure WC, resulting in ~99% density in 3 min. Both ZrB_2-based composites and pure WC produced by UHS are characterized by hardness values (15 and 21 GPa, respectively) similar to those reported in the literature for samples of comparable grain size (> 10 µm) produced by longer and more energy-consuming techniques.

CRediT authorship contribution statement

Emanuele De Bona: Conceptualization, Data curation, Investigation, Visualization, Writing – original draft. **Levent Karacasulu:** Investigation, Writing – original draft. **Cekdar Vakifahmetoglu:** Supervision, Writing – review & editing. **Vincenzo M. Sglavo:** Resources, Supervision, Writing – review & editing. **Mattia Biesuz:** Conceptualization, Methodology, Supervision, Writing – review & editing.

Declaration of Competing Interest

The authors declare the following financial interests/personal relationships which may be considered as potential competing interests: Vincenzo Sglavo reports financial support was provided by MISE. If there are other authors, they declare that they have no known competing financial interests or personal relationships that could have appeared to influence the work reported in this paper.

Data Availability

Data will be made available on request.

Acknowledgments

This work is supported by the Italian Ministry of Economic

Development (Ministero dello Sviluppo Economico, MISE) within the project “Processo Innovativo per la Ceramica Tecnica - PRINCE”, F/310085/01/X56. Levent Karacasulu acknowledges the support of TUBITAK (The Scientific and Technological Research Council of Türkiye) within 2214-A - International Research Fellowship Programme for PhD students.

Appendix A. Supporting information

Supplementary data associated with this article can be found in the online version at doi:10.1016/j.jallcom.2024.174102.

References

[1] J. Binner, M. Porter, B. Baker, J. Zou, V. Venkatachalam, V.R. Diaz, A. D'Angio, P. Ramanujam, T. Zhang, T.S.R.C. Murthy, Selection, processing, properties and applications of ultra-high temperature ceramic matrix composites, UHTCMCs – a review, Int. Mater. Rev. 65 (2020) 389–444, https://doi.org/10.1080/09506608.2019.1652006.

[2] L. Silvestroni, H.-J. Kleebe, W.G. Fahrenholtz, J. Watts, Super-strong materials for temperatures exceeding 2000 °C, Sci. Rep. 7 (2017) 40730, https://doi.org/10.1038/srep40730.

[3] W.G. Fahrenholtz, G.E. Hilmas, Ultra-high temperature ceramics: materials for extreme environments, Scr. Mater. 129 (2017) 94–99, https://doi.org/10.1016/j.scriptamat.2016.10.018.

[4] W.G. Fahrenholtz, E.J. Wuchina, W.E. Lee, Y. Zhou, Ultra-High Temperature Ceramics, Wiley, 2014, https://doi.org/10.1002/9781118700853.

[5] A.L. Chamberlain, W.G. Fahrenholtz, G.E. Hilmas, Pressureless sintering of Zirconium diboride, J. Am. Ceram. Soc. 89 (2006) 450–456, https://doi.org/10.1111/j.1551-2916.2005.00739.x.

[6] W.G. Fahrenholtz, G.E. Hilmas, S.C. Zhang, S. Zhu, Pressureless sintering of Zirconium diboride: particle size and additive effects, J. Am. Ceram. Soc. 91 (2008) 1398–1404, https://doi.org/10.1111/j.1551-2916.2007.02169.x.

[7] M. Thompson, W.G. Fahrenholtz, G. Hilmas, Effect of starting particle size and oxygen content on densification of ZrB2, J. Am. Ceram. Soc. 94 (2011) 429–435, https://doi.org/10.1111/j.1551-2916.2010.04114.x.

[8] S.-Q. Guo, Densification of ZrB2-based composites and their mechanical and physical properties: A review, J. Eur. Ceram. Soc. 29 (2009) 995–1011, https://doi.org/10.1016/j.jeurceramsoc.2008.11.008.

[9] W.G. Fahrenholtz, G.E. Hilmas, I.G. Talmy, J.A. Zaykoski, Refractory diborides of Zirconium and Hafnium, J. Am. Ceram. Soc. 90 (2007) 1347–1364, https://doi.org/10.1111/j.1551-2916.2007.01583.x.

[10] R. Telle, L.S. Sigl, K. Takagi, Boride-Based Hard Materials, in: Handb. Ceram. Hard Mater., Wiley-VCH Verlag GmbH, Weinheim, Germany, n.d.: pp. 802–945. https://doi.org/10.1002/9783527618217.ch22.

[11] E. De Bona, C. Manière, V.M. Sglavo, M. Biesuz, Ultrafast high-temperature sintering (UHS) of ZrB_2-based materials, J. Eur. Ceram. Soc. (2023), https://doi.org/10.1016/j.jeurceramsoc.2023.09.007.

[12] E. Zapata-Solvas, D.D. Jayaseelan, H.T. Lin, P. Brown, W.E. Lee, Mechanical properties of ZrB_2- and HfB2-based ultra-high temperature ceramics fabricated by spark plasma sintering, J. Eur. Ceram. Soc. 33 (2013) 1373–1386, https://doi.org/10.1016/j.jeurceramsoc.2012.12.009.

[13] S.C. Zhang, G.E. Hilmas, W.G. Fahrenholtz, Pressureless densification of Zirconium diboride with boron carbide additions, J. Am. Ceram. Soc. 89 (2006) 1544–1550, https://doi.org/10.1111/j.1551-2916.2006.00949.x.

[14] S. Zhu, W.G. Fahrenholtz, G.E. Hilmas, S.C. Zhang, Pressureless sintering of Zirconium diboride using boron carbide and carbon additions, J. Am. Ceram. Soc. 90 (2007) 3660–3663, https://doi.org/10.1111/j.1551-2916.2007.01936.x.

[15] E.W. Neuman, G.E. Hilmas, W.G. Fahrenholtz, Pressureless sintering of zirconium diboride with carbon and boron carbide nanopowder, Ceram. Int. 48 (2022) 13071–13079, https://doi.org/10.1016/j.ceramint.2022.01.183.

[16] S. Zhu, W.G. Fahrenholtz, G.E. Hilmas, S.C. Zhang, Pressureless sintering of carbon-coated zirconium diboride powders, Mater. Sci. Eng. A. 459 (2007) 167–171, https://doi.org/10.1016/j.msea.2007.02.116.

[17] S.K. Mishra, S.K. Das, A.K. Ray, P. Ramachandrarao, Effect of Fe and Cr addition on the sintering behavior of ZrB_2 produced by self-propagating high-temperature synthesis, J. Am. Ceram. Soc. 85 (2004) 2846–2848, https://doi.org/10.1111/j.1151-2916.2002.tb00540.x.

[18] D. Sciti, M. Brach, A. Bellosi, Oxidation behavior of a pressureless sintered ZrB_2–$MoSi_2$ ceramic composite, J. Mater. Res. 20 (2005) 922–930, https://doi.org/10.1557/JMR.2005.0111.

[19] D. Sciti, S. Guicciardi, A. Bellosi, G. Pezzotti, Properties of a pressureless-sintered ZrB_2-$MoSi_2$ ceramic composite, J. Am. Ceram. Soc. 89 (2006) 2320–2322, https://doi.org/10.1111/j.1551-2916.2006.00999.x.

[20] L. Silvestroni, D. Sciti, Effects of MoSi2 additions on the properties of Hf– and Zr–B_2 composites produced by pressureless sintering, Scr. Mater. 57 (2007) 165–168, https://doi.org/10.1016/j.scriptamat.2007.02.040.

[21] L. Silvestroni, G. Meriggi, D. Sciti, Oxidation behavior of ZrB_2 composites doped with various transition metal silicides, Corros. Sci. 83 (2014) 281–291, https://doi.org/10.1016/j.corsci.2014.02.026.

[22] L. Silvestroni, D. Sciti, F. Monteverde, K. Stricker, H. Kleebe, Microstructure evolution of a W-doped ZrB_2 ceramic upon high-temperature oxidation, J. Am. Ceram. Soc. 100 (2017) 1760–1772, https://doi.org/10.1111/jace.14738.

[23] F. Monteverde, A. Bellosi, Effect of the addition of silicon nitride on sintering behaviour and microstructure of zirconium diboride, Scr. Mater. 46 (2002) 223–228, https://doi.org/10.1016/S1359-6462(01)01229-5.

[24] H.-J. Ding, X.-G. Wang, J.-F. Xia, W.-C. Bao, G.-J. Zhang, C. Zhang, D.-Y. Jiang, Effect of solid solution and boron vacancy on the microstructural evolution and high temperature strength of W-doped ZrB_2 ceramics, J. Alloy. Compd. 827 (2020) 154293, https://doi.org/10.1016/j.jallcom.2020.154293.

[25] S.C. Zhang, G.E. Hilmas, W.G. Fahrenholtz, Pressureless Sintering of ZrB_2 –SiC Ceramics, J. Am. Ceram. Soc. 91 (2008) 26–32, https://doi.org/10.1111/j.1551-2916.2007.02006.x.

[26] P. Mazur, O. Grigoriev, D. Vedel, L. Melakh, I. Shepa, Ultra-high temperature ceramics based on ZrB_2 obtained by pressureless sintering with addition of Cr_3C_2, Mo_2C, and WC, J. Eur. Ceram. Soc. 42 (2022) 4479–4492, https://doi.org/10.1016/j.jeurceramsoc.2022.04.043.

[27] A. Khadimallah, X. Li, K. White, Solubility of tungsten in zirconium diboride solid solution, J. Eur. Ceram. Soc. 37 (2017) 1195–1203, https://doi.org/10.1016/j.jeurceramsoc.2016.11.039.

[28] J. Zou, G.-J. Zhang, S.-K. Sun, H.-T. Liu, Y.-M. Kan, J.-X. Liu, C.-M. Xu, ZrO_2 removing reactions of Groups IV–VI transition metal carbides in ZrB_2 based composites, J. Eur. Ceram. Soc. 31 (2011) 421–427, https://doi.org/10.1016/j.jeurceramsoc.2010.10.011.

[29] J. Zou, S.-K. Sun, G.-J. Zhang, Y.-M. Kan, P.-L. Wang, T. Ohji, Chemical reactions, anisotropic grain growth and sintering mechanisms of self-reinforced ZrB_2-SiC doped with WC, J. Am. Ceram. Soc. 94 (2011) 1575–1583, https://doi.org/10.1111/j.1551-2916.2010.04278.x.

[30] W.-M. Guo, Z.-G. Yang, G.-J. Zhang, High-temperature deformation of ZrB_2 ceramics with WC additive in four-point bending, Int. J. Refract. Met. Hard Mater. 29 (2011) 705–709, https://doi.org/10.1016/j.ijrmhm.2011.05.006.

[31] F. Monteverde, L. Silvestroni, Combined effects of WC and SiC on densification and thermo-mechanical stability of ZrB_2 ceramics, Mater. Des. 109 (2016) 396–407, https://doi.org/10.1016/j.matdes.2016.06.114.

[32] J. Zou, H.-B. Ma, A. D'Angio, G.-J. Zhang, Tungsten carbide: a versatile additive to get trace alkaline-earth oxide impurities out of ZrB_2 based ceramics, Scr. Mater. 147 (2018) 40–44, https://doi.org/10.1016/j.scriptamat.2017.12.033.

[33] J. Zou, G.-J. Zhang, C. Hu, T. Nishimura, Y. Sakka, J. Vleugels, O. Biest, Strong ZrB_2-SiC-WC ceramics at 1600°C, J. Am. Ceram. Soc. 95 (2012) 874–878, https://doi.org/10.1111/j.1551-2916.2011.05062.x.

[34] S.C. Zhang, G.E. Hilmas, W.G. Fahrenholtz, Oxidation of Zirconium diboride with Tungsten carbide additions, J. Am. Ceram. Soc. 94 (2011) 1198–1205, https://doi.org/10.1111/j.1551-2916.2010.04216.x.

[35] S.C. Zhang, G.E. Hilmas, W.G. Fahrenholtz, Improved oxidation resistance of Zirconium diboride by tungsten carbide additions, J. Am. Ceram. Soc. 91 (2008) 3530–3535, https://doi.org/10.1111/j.1551-2916.2008.02713.x.

[36] E.W. Neuman, M.J. Thompson, W.G. Fahrenholtz, G.E. Hilmas, Heating rate effects on the thermal and mechanical properties of ZrB_2, J. Am. Ceram. Soc. 105 (2022) 169–180, https://doi.org/10.1111/jace.18097.

[37] F. Monteverde, A. Bellosi, Beneficial effects of AlN as sintering Aid on microstructure and mechanical properties of hot-pressed ZrB_2, Adv. Eng. Mater. 5 (2003) 508–512, https://doi.org/10.1002/adem.200300349.

[38] F. Monteverde, A. Bellosi, S. Guicciardi, Processing and properties of Zirconium diboride-based composites, J. Eur. Ceram. Soc. 22 (2002) 279–288, https://doi.org/10.1016/S0955-2219(01)00284-9.

[39] G.J.K. Harrington, G.E. Hilmas, W.G. Fahrenholtz, Effect of carbon and oxygen on the densification and microstructure of hot pressed Zirconium diboride, J. Am. Ceram. Soc. 96 (2013) 3622–3630, https://doi.org/10.1111/jace.12561.

[40] L. Silvestroni, S. Failla, V. Vinokurov, I. Neshpor, O. Grigoriev, Core-shell structure: An effective feature for strengthening ZrB_2 ceramics, Scr. Mater. 160 (2019) 1–4, https://doi.org/10.1016/j.scriptamat.2018.09.024.

[41] L. Silvestroni, D. Sciti, TEM analysis, mechanical characterization and oxidation resistance of a highly refractory ZrB_2 composite, J. Alloy. Compd. 602 (2014) 346–355, https://doi.org/10.1016/j.jallcom.2014.02.133.

[42] E.W. Neuman, W.G. Fahrenholtz, G.E. Hilmas, Microstructure and mechanical properties of reaction-hot-pressed Zirconium diboride based ceramics, Int. J. Appl. Ceram. Technol. 16 (2019) 1715–1722, https://doi.org/10.1111/ijac.13263.

[43] F. Monteverde, R.J. Grohsmeyer, A.D. Stanfield, G.E. Hilmas, W.G. Fahrenholtz, Densification behavior of ZrB_2-$MoSi_2$ ceramics: The formation and evolution of core-shell solid solution structures, J. Alloy. Compd. 779 (2019) 950–961, https://doi.org/10.1016/j.jallcom.2018.11.238.

[44] W.-W. Wu, Z. Wang, G.-J. Zhang, Y.-M. Kan, P.-L. Wang, ZrB2–MoSi2 composites toughened by elongated ZrB_2 grains via reactive hot pressing, Scr. Mater. 61 (2009) 316–319, https://doi.org/10.1016/j.scriptamat.2009.04.013.

[45] H.-T. Liu, W.-W. Wu, J. Zou, D.-W. Ni, Y.-M. Kan, G.-J. Zhang, In situ synthesis of ZrB_2–MoSi2 platelet composites: reactive hot pressing process, microstructure and mechanical properties, Ceram. Int. 38 (2012) 4751–4760, https://doi.org/10.1016/j.ceramint.2012.02.061.

[46] J. Zou, H.-B. Ma, L. Chen, Y.-J. Wang, G.-J. Zhang, Key issues on the reactive sintering of ZrB_2 ceramics from elementary raw materials, Scr. Mater. 164 (2019) 105–109, https://doi.org/10.1016/j.scriptamat.2019.01.044.

[47] V. Zamora, A.L. Ortiz, F. Guiberteau, M. Nygren, Crystal-size dependence of the spark-plasma-sintering kinetics of ZrB_2 ultra-high-temperature ceramics, J. Eur. Ceram. Soc. 32 (2012) 271–276, https://doi.org/10.1016/j.jeurceramsoc.2011.08.027.

[48] V. Zamora, A.L. Ortiz, F. Guiberteau, M. Nygren, Spark-plasma sintering of ZrB2 ultra-high-temperature ceramics at lower temperature via nanoscale crystal refinement, J. Eur. Ceram. Soc. 32 (2012) 2529–2536, https://doi.org/10.1016/j.jeurceramsoc.2012.02.023.

[49] S. Grasso, T. Saunders, H. Porwal, O. Cedillos-Barraza, D.D. Jayaseelan, W.E. Lee, M.J. Reece, Flash spark plasma sintering (FSPS) of pure ZrB2, J. Am. Ceram. Soc. 97 (2014) 2405–2408, https://doi.org/10.1111/jace.13109.

[50] S. Mondal, J.D.S. Lombard, S. Gollapudi, C. Tallon, J. Li, D. Viehland, Ultrafast high-temperature sintering of ZrB 2, J. Am. Ceram. Soc. (2023), https://doi.org/10.1111/jace.19445.

[51] C. Wang, W. Ping, Q. Bai, H. Cui, R. Hensleigh, R. Wang, A.H. Brozena, Z. Xu, J. Dai, Y. Pei, C. Zheng, G. Pastel, J. Gao, X. Wang, H. Wang, J.-C. Zhao, B. Yang, X. (Rayne Zheng, J. Luo, Y. Mo, B. Dunn, L. Hu, A general method to synthesize and sinter bulk ceramics in seconds, Science 368 (80-) (2020) 521–526, https://doi.org/10.1126/science.aaz7681.

[52] S. Bhandari, C. Manière, F. Sedona, E. De Bona, V.M. Sglavo, P. Colombo, L. Fambri, M. Biesuz, G. Franchin, Ultra-rapid debinding and sintering of additively manufactured ceramics by ultrafast high-temperature sintering, J. Eur. Ceram. Soc. 44 (2024) 328–340, https://doi.org/10.1016/j.jeurceramsoc.2023.08.040.

[53] J. Wu, Y. Lin, C. Hu, S. Grasso, D. Zhu, J. Li, A. Katz-Demyanitcz, A. Goldstein, Ultra-fast high-temperature sintering of transparent MgAl2O4, Ceram. Int. 49 (2023) 19537–19540, https://doi.org/10.1016/J.CERAMINT.2023.03.018.

[54] T.P. Mishra, S. Wang, C. Lenser, D. Jennings, M. Kindelmann, W. Rheinheimer, C. Broeckmann, M. Bram, O. Guillon, Ultra-fast high-temperature sintering of strontium titanate, Acta Mater. 231 (2022) 117918, https://doi.org/10.1016/j.actamat.2022.117918.

[55] F. Zuo, Q. Wang, Z.Q. Yan, M. Kermani, S. Grasso, G.L. Nie, B.B. Jiang, F.P. He, H. T. Lin, L.G. Wang, Upscaling ultrafast high-temperature sintering (UHS) to consolidate large-sized and complex-shaped ceramics, Scr. Mater. 221 (2022) 114973, https://doi.org/10.1016/j.scriptamat.2022.114973.

[56] L. Spiridigliozzi, G. Dell'Agli, S. Esposito, P. Rivolo, S. Grasso, V.M. Sglavo, M. Biesuz, Ultra-fast high-temperature sintering (UHS) of Ce0.2Zr0.2Y0.2Gd0.2La0.2O2−δ fluorite-structured entropy-stabilized oxide (F-ESO), Scr. Mater. 214 (2022) 114655, https://doi.org/10.1016/j.scriptamat.2022.114655.

[57] A. Alemayehu, M. Biesuz, K.Y. Javan, A. Tkach, P.M. Vilarinho, V.M. Sglavo, V. Tyrpekl, Ultrafast high-temperature sintering of gadolinia-doped ceria, J. Eur. Ceram. Soc. 43 (2023) 4837–4843, https://doi.org/10.1016/j.jeurceramsoc.2023.04.025.

[58] Y. Sun, L. Zhao, R.-F. Guo, P. Shen, Cr3C2 assisted ultrafast high-temperature sintering of TiC, J. Eur. Ceram. Soc. 43 (2023) 5458–5465, https://doi.org/10.1016/j.jeurceramsoc.2023.05.031.

[59] R.-X. Luo, M. Kermani, Z.-L. Guo, J. Dong, C.-F. Hu, F. Zuo, S. Grasso, B.-B. Jiang, G.-L. Nie, Z.-Q. Yan, Q. Wang, Y.-L. Gan, F.-P. He, H.-T. Lin, Ultrafast high-temperature sintering of silicon nitride: a comparison with the state-of-the-art techniques, J. Eur. Ceram. Soc. 41 (2021) 6338–6345, https://doi.org/10.1016/j.jeurceramsoc.2021.06.021.

[60] H.-R. Mao, E.-T. Dong, S.-B. Jin, X.-M. Qiu, P. Shen, Ultrafast high-temperature synthesis and densification of high-entropy carbides, J. Eur. Ceram. Soc. 42 (2022) 4053–4065, https://doi.org/10.1016/j.jeurceramsoc.2022.03.054.

[61] R.-F. Guo, H.-R. Mao, P. Shen, Ultra-fast high-temperature synthesis and densification of high-entropy diborides and diboride-carbide ceramics, J. Eur. Ceram. Soc. 43 (2023) 5763–5773, https://doi.org/10.1016/j.jeurceramsoc.2023.05.042.

[62] B. Huang, L. Chen, S. Bai, Bulk ultrafine binderless WC prepared by spark plasma sintering, Scr. Mater. 54 (2006) 441–445, https://doi.org/10.1016/j.scriptamat.2005.10.014.

[63] V. Petříček, M. Dušek, L. Palatinus, Crystallographic computing system JANA2006: general features, Z. F. üR. Krist. Cryst. Mater. 229 (2014) 345, https://doi.org/10.1515/zkri-2014-1737.

[64] J.T. Norton, H. Blumenthal, S.J. Sindeband, Structure of diborides of titanium, zirconium, columbium, tantalum and vanadium, JOM 1 (1949) 749–751, https://doi.org/10.1007/BF03398932.

[65] K.D. Litasov, A. Shatskiy, Y. Fei, A. Suzuki, E. Ohtani, K. Funakoshi, Pressure-volume-temperature equation of state of tungsten carbide to 32 GPa and 1673 K, J. Appl. Phys. 108 (2010), https://doi.org/10.1063/1.3481667.

[66] J. Yang, F. Gao, First principles calculations of mechanical properties of cubic 5d transition metal monocarbides, Phys. B Condens. Matter 407 (2012) 3527–3534, https://doi.org/10.1016/j.physb.2012.05.016.

[67] T. Epicier, J. Dubois, C. Esnouf, G. Fantozzi, P. Convert, Neutron powder diffraction studies of transition metal hemicarbides M_2C_{1-x}—II. In situ high temperature study on W_2C_{1-x} and Mo_2C_{1-x}, Acta Met 36 (1988) 1903–1921, https://doi.org/10.1016/0001-6160(88)90293-3.

[68] E.J.W. Whittaker, (R. W. G.) Wyckoff Crystal Structures. Vol. 2. 2nd edn, New York, London, Sydney (Interscience Publishers), 1964. viii+588 pp. illus. Price: 180 s, Mineral. Mag. J. Mineral. Soc. 35 (1965) 554–555, https://doi.org/10.1180/minmag.1965.035.271.15.

[69] K. Aigner, W. Lengauer, D. Rafaja, P. Ettmayer, Lattice parameters and thermal expansion of $Ti(C_xN_{1-x})$, $Zr(C_xN_{1-x})$, $Hf(C_xN_{1-x})$ and TiN_{1-x} from 298 to 1473 K as investigated by high-temperature X-ray diffraction, J. Alloy. Compd. 215 (1994) 121–126, https://doi.org/10.1016/0925-8388(94)90828-1.

[70] A. Pak, A. Sivkov, I. Shanenkov, I. Rahmatullin, K. Shatrova, Synthesis of ultrafine cubic tungsten carbide in a discharge plasma jet, Int. J. Refract. Met. Hard Mater. 48 (2015) 51–55, https://doi.org/10.1016/j.ijrmhm.2014.07.025.

[71] A.S. Kurlov, A.I. Gusev, Tungsten carbides and W-C phase diagram, Inorg. Mater. 42 (2006) 121–127, https://doi.org/10.1134/S0020168506020051.

[72] C. Gasparrini, D. Rana, N. Le Brun, D. Horlait, C.N. Markides, I. Farnan, W.E. Lee, On the stoichiometry of zirconium carbide, Sci. Rep. 10 (2020) 6347, https://doi.org/10.1038/s41598-020-63037-0.

[73] H. Li, L. Zhang, Q. Zeng, J. Wang, L. Cheng, H. Ren, K. Guan, Crystal structure and elastic properties of ZrB compared with ZrB2: a first-principles study, Comput. Mater. Sci. 49 (2010) 814–819, https://doi.org/10.1016/j.commatsci.2010.06.027.

[74] Y. Champion, S. Hagege, Y. Champion, Structural analysis of phases and heterophase interfaces in the zirconium–boron system, J. Mater. Sci. 33 (1998) 4035–4041, https://doi.org/10.1023/A:1004470817744.

[75] V.G. Grebenkina, E.N. Denbnovetskaya, Thermal Coefficient of the Electrical Resistivity of Carbides and Their Solid Solutions, in: Refract. Carbides, Springer US, New York, NY, 1974, pp. 269–274, https://doi.org/10.1007/978-1-4684-8598-1_30.

[76] A. Nino, Y. Izu, T. Sekine, S. Sugiyama, H. Taimatsu, Effects of ZrC and SiC addition on the microstructures and mechanical properties of binderless WC, Int. J. Refract. Met. Hard Mater. 69 (2017) 259–265, https://doi.org/10.1016/j.ijrmhm.2017.09.002.

[77] G.-M. Song, Y.-J. Wang, Y. Zhou, The mechanical and thermophysical properties of ZrC/W composites at elevated temperature, Mater. Sci. Eng. A. 334 (2002) 223–232, https://doi.org/10.1016/S0921-5093(01)01802-0.

[78] F.W. Glaser, B. Post, System Zirconium-Boron, JOM 5 (1953) 1117–1118, https://doi.org/10.1007/BF03397597.

[79] R.H. Willens, E. Buehler, The superconductivity of the monocarbides of tungsten and molybdenum, Appl. Phys. Lett. 7 (1965) 25–26, https://doi.org/10.1063/1.1754239.

[80] P. Jia, L. Chen, J. Rao, Y. Wang, Q. Meng, Y. Zhou, Evolution of phase, microstructure and ZrC lattice parameter in solid-solution-treated W-ZrC composite, Sci. Rep. 7 (2017) 6531, https://doi.org/10.1038/s41598-017-06301-0.

[81] P. Sengupta, S. Basu, I. Manna, Comparative evaluation of TiC and/or WC addition on microstructure, mechanical properties, thermal residual stress and reciprocating wear behaviour of ZrB_2–20SiC composites, J. Mater. Sci. 58 (2023) 420–442, https://doi.org/10.1007/s10853-022-08021-x.

[82] P. Sengupta, S.S. Sahoo, A. Bhattacharjee, S. Basu, I. Manna, Effect of TiC addition on structure and properties of spark plasma sintered ZrB_2–SiC–TiC ultrahigh temperature ceramic composite, J. Alloy. Compd. 850 (2021) 156668, https://doi.org/10.1016/j.jallcom.2020.156668.

[83] P. Sengupta, S. Basu, I. Manna, Effect of TiC reinforcement on densification, structural evolution and high-temperature oxidation behaviour of ZrB_2-20 vol pct SiC composite, Metall. Mater. Trans. A 54 (2023) 1252–1270, https://doi.org/10.1007/s11661-023-06982-5.

[84] D.-L. Hu, H. Gu, J. Zou, Q. Zheng, G.-J. Zhang, Core−rim structure, bi-solubility and a hierarchical phase relationship in hot-pressed ZrB_2−SiC−MC ceramics (M=Nb, Hf, Ta, W), J. Mater. 7 (2021) 69–79. https://doi.org/10.1016/j.jmat.2020.07.005.

[85] B. Post, F.W. Glaser, D. Moskowitz, Transition metal diborides, Acta Met. 2 (1954) 20–25, https://doi.org/10.1016/0001-6160(54)90090-5.

[86] R.W. Harrison, W.E. Lee, Processing and properties of ZrC, ZrN and ZrCN ceramics: a review, Adv. Appl. Ceram. 115 (2016) 294–307, https://doi.org/10.1179/1743676115Y.0000000061.

[87] M. Usta, M. Ipek, C. Bindal, The characterization of borided pure tungsten, Surf. Coat. Technol. (2005) 6–11, https://doi.org/10.1016/j.surfcoat.2004.06.042.

[88] E. Rudy, S. WindischTernary phase equilibria in transition metal-boron-carbon-silicon systems 615 (33 Part Ii. Ternary Syst. Vol. XIII Phase Diagr. Syst. Ti-B-C., Zr-B-C. Hf-B-C. Ternary Phase Equilibria Transit. Met. Syst. Rep. No. AFMLTR-65-2. Contract No. USAF,1966, ⟨https://www.scopus.com/inward/record.uri?eid=2-s2.0-84928823411&partnerID=40&md5=56a8d6007b05957ebf573074a8476fd9⟩, pp. 183-188.

[89] E. Rudy, Ternary Phase Equilibria in Transition Metal-boron-carbon-silicon Systems: Part V. Compendium of Phase Diagram Data, Air Force Materials Laboratory USA, 1969.

[90] W.-M. Guo, L.-X. Wu, Y. You, H.-T. Lin, G.-J. Zhang, Three-step reactive hot pressing of B4C–ZrB2 ceramics, J. Eur. Ceram. Soc. 36 (2016) 951–957, https://doi.org/10.1016/j.jeurceramsoc.2015.11.022.

[91] Y. Chen, D. He, J. Qin, Z. Kou, Y. Bi, Ultrasonic and hardness measurements for ultrahigh pressure prepared WB ceramics, Int. J. Refract. Met. Hard Mater. 29 (2011) 329–331, https://doi.org/10.1016/j.ijrmhm.2010.12.006.

[92] H.O. Pierson, Carbides of Group IV. Titanium, Zirconium, and Hafnium Carbides, William Andrew Publishing, Westwood, NJ, 1996, pp. 55–80, 410.1016/B978-081551392-6.50005-2N.Pierson.

[93] A.L. Chamberlain, W.G. Fahrenholtz, G.E. Hilmas, D.T. Ellerby, High-strength Zirconium diboride-based ceramics, J. Am. Ceram. Soc. 87 (2004) 1170–1172, https://doi.org/10.1111/j.1551-2916.2004.01170.x.

[94] J.J. Swab, J. Jarman, W. Fahrenholtz, J. Watts, Mechanical properties of ZrB_2 ceramics determined by two laboratories, Int. J. Appl. Ceram. Technol. (2023), https://doi.org/10.1111/ijac.14429.

[95] S. Mandal, S. Chakraborty, P. Dey, A study of mechanical properties and WEDM machinability of spark plasma sintered ZrB_2–B4C ceramic composites, Micron 153 (2022) 103198, https://doi.org/10.1016/j.micron.2021.103198.

[96] A.N. Dorner, K. Werbach, G.E. Hilmas, W.G. Fahrenholtz, Effect of tantalum solid solution additions on the mechanical behavior of ZrB_2, J. Eur. Ceram. Soc. 41 (2021) 3219–3226, https://doi.org/10.1016/j.jeurceramsoc.2020.12.049.
[97] L. Chen, Y. Lei, J. Zhang, J. Wang, Synthesis and characterization of ZrCx coatings with different stoichiometry, Vacuum 202 (2022) 111211, https://doi.org/10.1016/j.vacuum.2022.111211.
[98] Y. Wang, D. Zhu, X. Jiang, P. Sun, Binderless sub-micron WC consolidated by hot pressing and treated by hot isostatic pressing, J. Ceram. Soc. Jpn. 122 (2014) 329–335, https://doi.org/10.2109/jcersj2.122.329.